ANALYSIS OF IONOSPHERIC ANOMALIES DUE TO SPACE WEATHER CONDITIONS BY USING GPS-TEC VARIATIONS

Mustafa ULUKAVAK and Mualla YALCINKAYA, Turkey

Key words: Ionosphere, Space Weather Condition, Geomagnetic Storm, Solar Activity, GPS-TEC

SUMMARY

The Global Positioning System (GPS) is used as an important tool for ionosphere monitoring and obtaining the Total Electron Content (TEC) variations. GPS satellites, positioned in the Earth's orbit, are used as sensors to investigate the space weather conditions. In this study, changes in the ionospheric TEC, which originated from space weather conditions (Solar and geomagnetic activities), were investigated at different time periods and latitudes around the world. GPS observations used to obtain GPS-TEC variations were obtained from International GNSS Service (IGS) stations at North and South Regions (equatorial and mid-latitude). The GPS-TEC changes obtained from the GPS observations of each IGS station were analyzed using the quartile-based statistical analysis (15-day running median) method. This study was carried out to determine the ionospheric TEC anomalies originating from different space weather conditions at different times in a total of 28 different regions selected at equatorial and mid-latitude regions. Instantaneous GPS-TEC variations are revealed by using 15-day running median statistical analysis method with examining the solar and geomagnetic activity indices. The investigations revealed that it is possible to use the GPS-TEC for monitoring the space weather conditions. This study is supported by TUBITAK CAYDAG grant no. 116Y109.

ANALYSIS OF IONOSPHERIC ANOMALIES DUE TO SPACE WEATHER CONDITIONS BY USING GPS-TEC VARIATIONS

Mustafa ULUKAVAK and Mualla YALCINKAYA, Turkey

1. INTRODUCTION

The atmospheric layer surrounding the Earth is composed of 99% Nitrogen (N_2) and Oxygen (O_2) and Carbon Dioxide (CO_2) and other gaseous structures (Rishbeth and Garriott, 1969; Ratcliffe, 1972) The atmosphere of the Earth is divided into various layers depending on the activity of the Sun, the gravity and magnetic field of the Earth, the temperature and the degree of ionization. Depending on the temperature, it is divided into troposphere, stratosphere, mesosphere, thermosphere and exosphere. The ionosphere layer, which depends on the degree of ionization, is divided into a neutral ionosphere up to 70 km in height, a plazma up to 1000 km in height from 70 km and a magnetosphere. It is a layer about 50 - 350 km in height, including the ionosphere, the mesosphere and the thermosphere. This layer is called the ionosphere because the sun's rays (ultraviolet- and gamma-rays) on the topmost layer of the atmosphere ionize a significant portion of the neutral air molecules. The understanding of the ionosphere layer as a conductive layer on the upper part of the atmosphere lasts about a century ago. The idea that a conductive layer influenced by magnetic field changes in the atmosphere was introduced by Gauss in 1839 and by Kelvin in 1860. Taylor in 1903 and Fleming in 1906 stated that this layer was affected by the sun's rays. The fully ionospheric concept was developed a few years after the discovery of Thomson's electrons (Ratcliffe 1972). In general, ionosphere; (Wild, 1994), and may show changes in geographical location, geomagnetic location, geomagnetic activity, solar activity, number of sunspots, seasonality, local time, nuclear explosions, strong lightning and severe storms (Liu et al., 2014; Vellinov et al., 1992; Hawarey and Ayan, 2004).

Daytime Extreme ultraviolet (EUV) rays and X-rays emitted from the sun multiply atoms and molecules that are gaseous in the atmosphere, causing positively charged ions and negatively charged free electrons to form, that is, to undergo photoionization (Ratcliffe, 1972). In the hours when the sun is not visible, ions and electrons recombine to form neutral atoms and molecules, causing backward inverse operations in the ionosphere. The electron density is effected by the geographical and geomagnetic location, the solar activity, the geomagnetic activity, the seasonality, the local time and the altitude, which are the most important parameters in the ionosphere, show the quantity of electrons in the unit volume. Photoionization affects the change in electron-ion concentration with different processes in the ionosphere (Prölss, 2004).

Due to solar and/or geomagnetic activity, time-dependent changes in the Solar System, including the magnetosphere, ionosphere, and thermosphere conditions, form the space weather conditions. Solar activities can affect Earth's space weather conditions in three different ways. The first is the CME-Coronal Mass Ejections, which radiate extreme hot plasma to the space gap, the second is the high-velocity plasma released from the crown holes forming the Sun winds, and the third is the Sun bursts of magnetic energy released with intense radiation (URL-1, 2014). The influence of the ionosphere layer causes major changes such as changing the

density distribution in the ionosphere, increasing or decreasing the TEC values, and impairing the current balance in the ionosphere (Komjathy, 1997). In order to model these changes in the ionosphere, it is necessary to define the solar activity and/or geomagnetic indices and determine the solar and geomagnetic effect levels. In order to interpret the solar and geomagnetic activities that cause the change in the ionosphere, indices called as variables of space weather conditions are used. Space weather condition indices can be defined by observing continuously with terrestrial or spatial devices. Indicators such as solar activity, geomagnetic storm and geomagnetic activity, magnetic field, plasma density and particle flux are used to determine space weather conditions (Ratcliffe, 1972).

In this study, changes in the ionospheric TEC, which originated from space weather conditions (Solar and geomagnetic activities), were investigated at different time periods and latitudes around the world. GPS observations used to obtain GPS-TEC variations were obtained from International GNSS Service (IGS) stations at North and South Regions (equatorial and mid-latitude). The GPS-TEC changes obtained from the GPS observations of each IGS station were analyzed using the quartile-based statistical analysis (15-day running median) method. This study was carried out to determine the ionospheric TEC anomalies originating from different space weather conditions at different times in a total of 28 different regions selected at equatorial and mid-latitude regions. Section 2 describes the space weather condition indices, Section 3 explains the derivation of the GPS-TEC data from GNSS observations and analysis of the daily GPS-TEC variations, and Section 4 explains the analysis of the space weather condition activities and GPS-TEC analysis results. The conclusions are given in Section 5.

2. SPACE WEATHER CONDITION INDICES

2.1 Solar Activity Indices

F10.7 indice, which is the most commonly used indice showing the level of solar activity, allows the measurement of the amount of UV and X-rays emitted from the sun. It is used to investigate the changes that solar activities bring to the ionosphere. The solar flux is directly related to the number of sunspots. Assuming that the F10.7 indices with two different scales are smaller than 150sfu, poor solar activity is considered high solar activity when it is larger than 150sfu (Vitinsky et al., 1986). Solar flux indice data can be obtained in eight hours resolution from the web page (URL-8, 2014) of the NASA Goddard Space Flight Center's Space Physics Data Facility.

The Extreme Ultraviolet Energy (EUV) indice covers the electromagnetic spectrum of the solar radiation in the 0.1-120 nm wavelength. These high-energetic particles affect the upper atmosphere, where they are absorbed so that the ionosphere is not only heated but also photo-ionized. The EUV photons reaching the Earth are also completely absorbed by the upper atmosphere at an altitude of about 80 km. EUV photons ionize the atmosphere and provide ionosphere by the formation of electrons (Tobiska, 1996). Since the sun's EUV radiation is completely absorbed by the upper atmosphere, it is impossible to measure it from the ground. These measurements must be made either by satellites or rockets directly outside the atmosphere. At times when EUV measurements could not be made to determine solar activity,

scientists used the number of sunspots and the indice of solar flux F10.7 cm (URL-6, 2014). Solar EUV Monitoring (SEM) has been carried out by the Solar Heliospheric Observatory (SOHO) satellite since 1996, at 26-34 nm and 0.1-50 nm wavelength bands (Judge et al., 1998). Values for EUV indices can be retrieved daily from the Internet interface of the University of Southern California's Space Science Center (URL-7, 2014).

2.2 Geomagnetic Storm and Geomagnetic Activity Indices

Disturbances caused by geomagnetic storms also affect the high frequency GPS signals passing through the ionosphere layer, forming the source of error modeling of ionosphere (Zolesi and Cander, 2014). This causes a deterioration by affecting the global electric current (GEC) variability (URL-5, 2014). These effects are characterized by indices, where active changes from space and Earth stations are measured and assessed, include geomagnetic storm (Kp) and geomagnetic activity (Dst) indices.

The Kp-indice, which is the indice of the geomagnetic storm, is a useful indicator for the announcement of warnings and warnings in the determination of Earth's magnetic field and geomagnetic changes. The Kp indice values are determined by the NOAA Space Weather Prediction Center, measured from 13 magnetometer stations located between the north and south latitudes, 44^o and 60^o. The Kp-indice, which ranges from 0 to 9, uses the horizontal component of the Earth's magnetic field in determining the scale (De Canck, 2007). Data from the geomagnetic storm indice can be acquired in one hour resolution from the Nasa Goddard Space Flight Center (SPDF) spacefic data facility's (URL-8, 2014) internet interface. The scale values of the Kp-indice are determined by the change of the geomagnetic field and the geomagnetic storm effect in the nanoTesla (nT) unit.

The Dst-indice is a geomagnetic indicator that identifies the magnetic flux changes in the equatorial regions and the measurements are taken by the magnetometers placed in the equatorial regions (Zolesi and Cander, 2014). The Dst-indice measurements obtained as an hourly average of the magnetic shaking were evaluated by the Geomagnetism and Space Magnetism Data Analysis Center of the Institute of Science, Kyoto University in Japan, and the NASA Goddard Space Flight Center's Space Physics Data Facility (URL-8, 2014) is published as an hour resolution from the web interface. Geomagnetic activity indice boundaries classified by five different scales by Loewe and Prölss (1997) were then classified into three different scales by Kamide et al. (1998), Rozhnoi et al., (2004) and Contadakis et al., (2012).

2.3 Magnetic Field Change Indices

The Earth's magnetic field shows similar behavior of the magnetic field of the bar magnet. Under the influence of solar winds, these magnetic field lines are compressed in the direction of the sun and extend in the direction of the wind. This effect forms the special shape of the magnetosphere around the Earth called the tear drop. The interplanetary magnetic field is the influence of the magnetic fields of the plasma gushes coming from the solar corona and the domain of the Sun, the two main components of the thought high-speed solar propagation. The magnetic field of the Sun, which resembles the magnetic field of the Earth, also comes close to

each other in the poles but the equatorial line is distant from each other (Aschwanden, 2005). These places where the magnetic field lines are concentrated are referred to as twin poles (dipoles). But Earth's magnetic field is 100 times smaller than the Sun's. As the sun's activity reaches its peak, many sunspots become visible on the sun's bright disc. In this case, the sunspots are filled with magnetism and large magnetic field lines, and sputtering of matter is detected (Gonzalez et al., 1994). Interplanetary magnetic field indices (Bx, By and Bz) are expressed as vector quantities and two components (Bx and By) are parallel to the plane of orbits, and the third component (Bz) perpendicular to the plane of orbits.
The Bz component of the magnetic field turns south in the initial phase of the magnetic storm while the north side is in calm day conditions (Abraha 2014). Under quiet conditions, the E × B rotation occurs in the west direction, with the electric field (E) and the magnetic field (B) in the By field of the electric field. Generally, when the magnetic disturbances occur, it decreases (in equatorial regions) and this leads to a decrease in the downward slip (positive value to negative value), resulting in a positive phase. However, in the case of severe deterioration, an increase in downward slip is observed in By, with the negative phase of the storm emerging (Turunen and Rao 1980, Adeniyi 1986). The extra plasma production, however, leads to the expansion of the F2 layer. Loewe and Prölss (1997) classified the magnetic activity indice limit values classified on five different scales into three different scales by Gonzalez et al. (1994). Magnetic field indice data is available as a one-hour resolution from the web interface of the NASA Goddard Space Flight Center's Space Physics Data Facility (URL-8, 2014)

2.4 Plasma Density and Particle Flux Indices

The plasma density, the protons carried by the radiation storms, is directed by the Earth's magnetic field and collides in the north and south poles in the upper atmosphere. Fast-moving protons display the same effect as X-ray photons and expand in the D-layer of the ionosphere and interfere with high-frequency signal communication at high latitudes. Electrons decaying during auroral effects increase in other layers and create interferences (parasites) in signal transmission (URL-3, 2014). The unit of plasma density is given as the proton density (Np/cm^3) and the number of protons passing through the unit cubic centimeter volume (URL-4, 2014). In the slow solar winds, the value of the density of proton increases, while it decreases in the fast solar winds (Schwenn, 2001). 15 protons/cm^3 in the proton density in Dashora et al. (2009) are larger than +5 nT (weak storm) or -5 nT (weak storm) have been shown to be in direct contact with the situation. For this reason, proton density indice values greater than 15 proton/cm^3 are evaluated as active space weather conditions. The data for the density of the proton density can be obtained in one hour resolution from the web interface of the NASA Goddard Space Flight Center's Space Physics Data Facility (URL-8, 2014).
Particle flux is detected by the amount of energetic particles (protons) that are emitted by the effects of solar explosions and interplanetary magnetic field (Melnikov, 1990). Energy intensive particles are evaluated at six energy thresholds (1, 2, 4, 10, 30 and 60 MeV: Million Electro Volt) (URL-2, 2014). Melnikov (1990) has revealed a correlation between microwave propagation and >10 MeV proton flux. The energy unit of the charged particles identified in the MeV unit shows the amount of energy of the protons in the proton flux unit (pfu). The

particle flux (10 pfu) is carried out by detecting the number of protons (10 pfu = 10 proton cm^{-2} $sr^{-1}s^{-1}$) passing in one second (defined as a curved surface) at a steradian angle (cm^2) (Schwenn, 2001). Particle flux indices can be acquired in one hour resolution from the NASA Goddard Space Flight Center's Space Physics Data Facility's (URL-8, 2014) web interface.

3. GPS-TEC AND ANALYSIS OF TEC VARIATIONS

3.1 Obtaining TEC Data From GNSS Observations

Changes in ionospheric TEC can be determined by GNSS data. The geometry-free linear combination of the code (P) or carrier-phase (Φ) measurements can be used to estimate the ionospheric TEC. The geometry free linear combination for pseudo-range measurements can be calculated by subtracting the measurements of the P_2 code from the P_1 code:

$$P_{4,u}^{m} = P_1 - P_2 = A\left(\frac{1}{f_1^2} - \frac{1}{f_2^2}\right) STEC_u^m + DCB^m + DCB_u \quad (1)$$

where f_1 and f_2 are the carrier frequencies of L1 and L2 signals of GPS satellites. A ($40.3\, m^3/s^2$) and $STEC_u^m$ indicate the Slant Total Electron Content (STEC) in units of TECU ($1\ \text{TECU} = 10^{16}\text{electrons/m}^2$) on the slant signal path combining the receiver u and satellite m. DCB^m and DCB_u are the differential code biases (DCBs) defined for pseudo-range measurements. The geometry-free linear combination for carrier-phase measurements can be obtained by subtracting the measurements of the Φ_2 phase from the Φ_1 phase:

$$\Phi_{4,u}^{m} = \Phi_1 - \Phi_2 = -A\left(\frac{1}{f_1^2} - \frac{1}{f_2^2}\right) STEC_u^m + IFB^m + IFB_u + \Delta N_{u,4}^m \quad (2)$$

where, IFB^m and IFB_u are the inter-frequency biases for the carrier-phase measurements for satellite and receiver, respectively. The combined ambiguity term $\Delta N_{u,4}^m$ in equation (2) is defined as follows:

$$\Delta N_{u,4}^m = \lambda_1 \mathrm{N}_{u,1}^m - \lambda_2 \mathrm{N}_{u,2}^m \quad (3)$$

where $\mathrm{N}_{u,1}^m$ and $\mathrm{N}_{u,2}^m$ show the integer phase ambiguities, and λ_1, λ_2 are the wavelengths corresponding the to f_1 and f_2 frequencies, respectively.

DCBs should be determined to obtain unbiased STEC. However, a standard procedure on how to include these DCBs into TEC computation has yet to be determined (Komjathy 1997). DCBs are eliminated in STEC calculation as follows:

$$STEC_u^m(n) = \frac{1}{A}\left(\frac{f_1^2 f_2^2}{f_2^2 - f_1^2}\right)\left[P_{4,u}^m(n) - (DCB^m + DCB_u)\right] \quad (4)$$

where indice n denotes the time sample ranges from 1 to N (total number of time samples in a record). N obtains the value 2880 for 24-hour continuously observation with 30 seconds of sampling interval. The Φ_4 data are usually fitted to P_4 using various algorithms to obtain carrier-phase measurements with low noise (Lanyi and Roth 1988). Each cycle- slip or phase discontinuity is used for another constant offset calculation. The leveling or fitting of Φ_4 to P_4 is completed by defining a constant offset for each continuous arc of phase measurements:

$$B^m = \frac{1}{N_{me}} \sum_{n_{me}=1}^{N_{me}} \left(P_{4,u}^m(n_{me}) + \Phi_{4,u}^m(n_{me}) \right) \quad (5)$$

where B^m is the constant offset value for the m^{th} satellite; N_{me} is the total number of samples in each continuous phase arc; n_{me} is the time duration of the total samples in each continuous phase arc. STEC is determined by combining the constant offset value B^m and Φ_4 in equation (6) to obtain the following:

$$STEC_u^m(n) = \frac{1}{A}\left(\frac{f_1^2 f_2^2}{f_2^2 - f_1^2}\right)\left(B^m - \Phi_{4,u}^m(n) - (DCB^m + DCB_u)\right) \quad (6)$$

VTEC can be obtained using a thin shell approximation (Klobuchar 1986) of the single layer ionosphere model for which the relation between STEC and VTEC is given as follows:

$$M\left(z_m(n)\right) = \frac{STEC_u^m(n)}{VTEC_u^m(n)} \quad (7)$$

where the mapping function $z_m(n)$ is defined as the satellite zenith angle at the receiver position. The mapping function $M(z)$ is defined as follows:

$$M(z) = \frac{1}{cosz'} = \frac{1}{\sqrt{1 - sin^2\, z'}}\ ,\ sinz' = \frac{R}{R+H}\sin(\alpha z) \quad (8)$$

where, z' is the zenith angle at the ionospheric pierce point (IPP) where the line-of-sight between the satellite and ground receiver intersects the thin shell. R is the earth radius (6,378.137 km), $\alpha = 0.9886$ is a scaling factor from the modified single layer mapping function (Schaer 1999) and H is the ionospheric shell height 350 km.

The DCBs of the satellites and receivers are available from the daily IGS IONEX files. The unknown DCB values at the receivers can also be predicted as daily constants by using the regional VTEC modeling based on spherical harmonic functions. The order of spherical harmonics expansion depends on the areas; for instance, 4th, 8th, and 15th order for the regional, continental, and global size, respectively (Jin *et al.* 2012).

The calibrated STEC variations are obtained by removing the estimated DCBs from each satellite arc in equation (6). The VTEC values are determined using equation (7) for each continuous arc. The hourly VTEC values are determined using the selected IPP point and VTEC values obtained through the surface coefficients of the polynomials at an appropriate data window. In this study, the hourly VTEC values are estimated with the calibrated VTEC values at IPP over each GNSS station by fitting the approximation of second-order polynomial surfaces to IPP points for a 24-hour run (Durmaz and Karslioglu 2014).

$$VTEC(\varphi_{IPP}, s_{IPP}) = a_0 + a_1\varphi_{IPP} + a_2 s_{IPP} + a_3{\varphi_{IPP}}^2 + a_4\varphi_{IPP}s_{IPP} + a_5{s_{IPP}}^2 \qquad (9)$$

where φ_{IPP} and s_{IPP} are the spherical coordinates of the IPP in the sun-fixed reference frame; a_0, a_1, a_2, a_3, a_4 and a_5 are the polynomial surface coefficients. The hourly unknown polynomial surface coefficients are estimated using least-squares estimation. The topside hourly VTEC values at each station are calculated by substituting the sun-fixed spherical coordinates of each station alongside the estimated polynomial surface coefficients in equation (9). Insufficient data will reveal problems in estimating the hourly VTEC value. However, the missing VTEC values above the stations should also be completed by interpolating the grid TEC data obtained from IGS IONEX files.

3.2 Analysis of Daily GPS-TEC Variations

Investigation on the space weather conditions ionospheric VTEC anomalies can be performed by using 15-day moving median (MM) methods that employ the quartile based statistical analysis method (Liu et al. 2009). The MM values of GPS-TEC were calculated in advance by using the quartile-based statistical analysis method. The lower quartile (LQ) and upper quartile (UQ) were also calculated. Assuming that the GPS-TEC values are in the normal distribution with mean (m) and standard deviation (σ), the expected values of MM and LQ or UQ are m and 1.34 σ, respectively (Klotz and Johnson 1983). The lower bound (LB) and upper bound (UB) are calculated as LB=MM-1.5(MM-LQ) and UB=MM+1.5(UQ-MM), respectively. Anomalous variations can be detected in observed GPS-TEC greater than UB or lesser than the associated LB (Liu *et al.* 2009). For example, the VTEC values for the first 15 days were used to generate MM, UB and LB for the 16th day. Similarly, 15 days of VTEC data between the 2nd and 16th day are used to generate bounds for the 17th day. If more than one- third of the data (e.g., eight hours are anomalous in a day) are greater or lesser than these UBs and LBs in a day, this day is taken as anomalous.

4. RELATIONS BETWEEN SPACE WEATHER CONDITION INDICES AND GPS-TEC ANALYSIS RESULTS

4.1 Analysis Result of Space Weather Conditions

The geomagnetic storm and geomagnetic activity indices (Kp and Dst), magnetic field indices (Bx, By and Bz), plasma density, and magnetic field indices (F10.7cm and EUV 0.1-50nm,

EUV 26-34nm) time series of these data were generated and analyzed after the particle stream indices (proton density and proton flux at six different energy levels) were obtained for all regions. As an example, time series of space weather conditions between 5 March - 3 May 2010 were given and analyzed. Time series (Figure 1) for solar activity indice indices (F10.7cm and EUV 0.1-50nm, EUV 26-34nm) from space weather conditions were determined and analyzed.

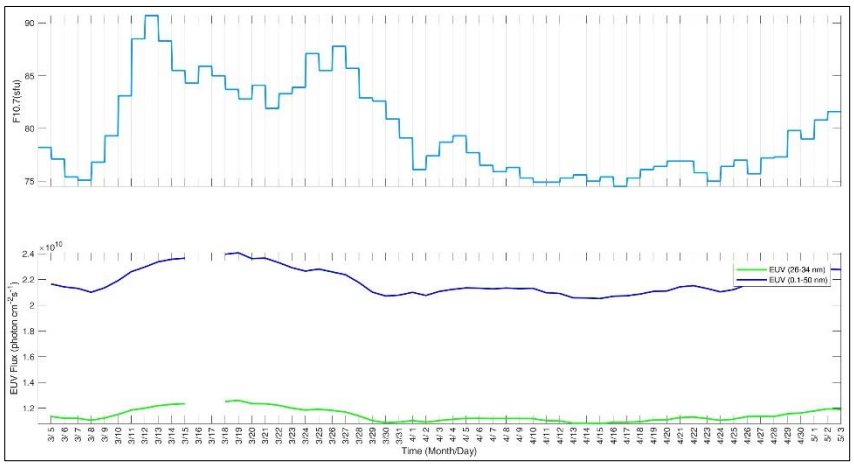

Figure 1. Solar Activity Indices (F10.7cm and EUV 0.1-50nm, EUV 26-34nm)

When the indice values of the solar activity changes in Figure 1 are examined, F10.7cm is seen that the changes of the solar flux indice are lower than the 150 SFU which is the boundary value. Changes in EUV (0.1-50 nm) and EUV (26-34 nm) indices were found to have data losses on the 16th and 17th March. However, these days were not taken into consideration as TEC anomalies remained within the first 15 days of 15-day moving median statistical analysis. Time series of geomagnetic storm and geomagnetic activity indices (Kp and Dst) were created from space weather conditions (Figure 2) and analyzed.

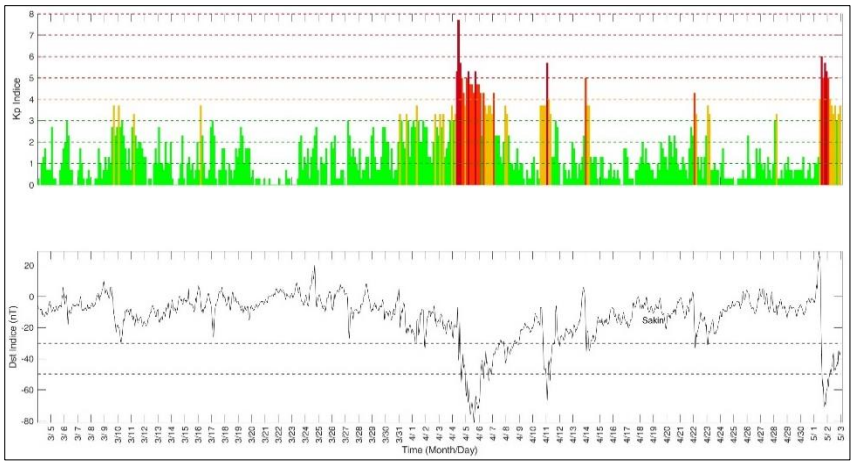

Figure 21. Geomagnetic Storm and Geomagnetic Activity Indices (Kp and Dst)

When the indice values of the geomagnetic storm (Kp) and geomagnetic activity (Dst) changes in Figure 2 are examined, Kp indice values did not exceed the 4 Kp limit value. The geomagnetic activity (Dst) indices (-50 nT) did not exceed the threshold value. Time series (Figure 3) of the magnetic field indices (Bx, By and Bz) from the space weather conditions are drawn and analyzed.

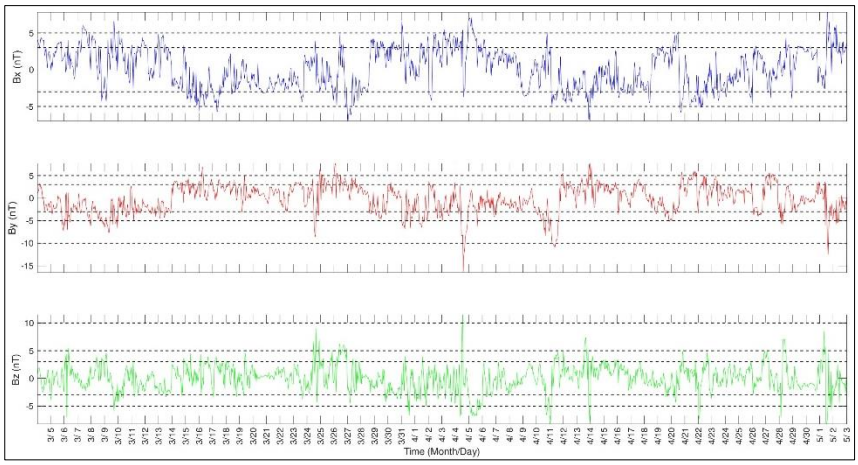

Figure 3. Magnetic Field Indices (Bx, By and Bz)

Changes in the magnetic field indices (Bx, By and Bz) were found to exceed the limit values of +5 and -5 nT. Time series of plasma density and particle flux indices were plotted (Figure 4) and analyzed.

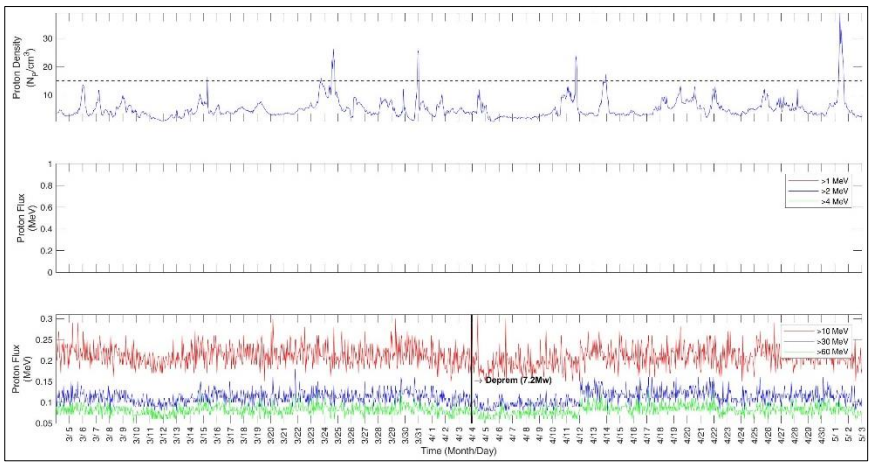

Figure 4. Plasma density and particle flux indices

All indices in Figures 1, 2, 3, and 4 are examined together to determine the days when the indices peaked and exceeded (active days (A)) the threshold value and are shown as (+). The "calm day (C)" decision was made for days not peaking or exceeding the limit values of the

indice values. All indices were evaluated for each selected region for analysis. However, in order to get a clearer picture of the results, the charts were only shown for 20 days (Table 1).

Table 1. Analysis of space weather conditions in in 2010

Time (Month/Day)		3/20	3/21	3/22	3/23	3/24	3/25	3/26	3/27	3/28	3/29	3/30	3/31	4/1	4/2	4/3	4/4	4/5	4/6	4/7	4/8	4/9
	F10.7		+				+		+									+				+
	EUV(.1-50nm)		+				+							+				+				+
	EUV(26-34nm)		+				+							+				+				+
	Kp																	+	+	+		
	Dst (nT)																	+	+	+		
	Bx (nT)								+					+				+	+			
	By (nT)						+	+	+					+	+			+	+			
	Bz (nT)						+		+					+				+	+			
	N_P					+	+															
	>1MeV																					
	>2MeV																					
	>4MeV																					
	>10MeV																					
	>30MeV																					
	>60MeV																					
DECISION		C	A	C	C	A	A	A	A	C	C	C	C	A	A	C	C	A	A	A	C	A

As shown in Table 1, active and calm days were determined according to the space weather conditions.

4.2 Analysis Results of GPS-TEC Variations

In order to test the reliability of the calculated VTEC values of the IGS stations, the VTEC values of the GIM-TEC maps were compared with the estimated VTEC values. Daily averages and standard deviations of the VTEC values calculated for this purpose and the VTEC values from the IGS IONEX files were calculated for each IGS station and given as an example for the year 2010. The correctness of the TEC values in the IGS IONEX files is defined in 2-8 TECU intervals on the continents (URL-9, 2014). Estimated VTEC values can be considered reliable. Abnormal changes in VTEC values after reliability of predicted VTEC values have been tested by Liu et al. (2009) is based on a statistical analysis of the difference between quarters with a similar algorithm.

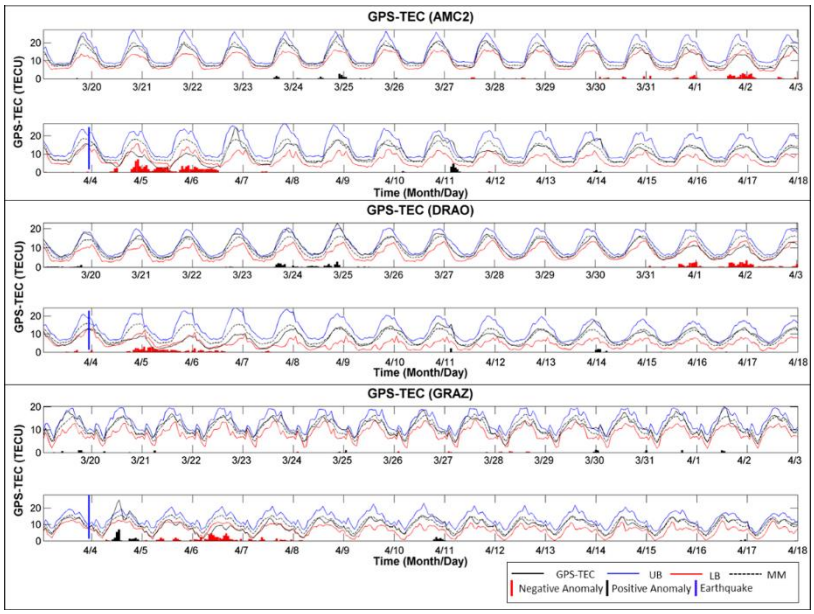

Figure 5. VTEC values of IGS stations in 2010

To determine the days when VTEC changes were abnormal, the percentages of the low or high numbers of LB or UB of a day's hourly VTEC changes were determined with software prepared in the MATLAB environment. VTEC change percentages (>8/24hrs) of abnormal days determined from selected IGS points for each region were calculated and the results of the space weather conditions were evaluated as negative abnormal day with a calm day decision VTEC change percentages are pink, positive abnormal days VTEC change percentages are in gray colors for year the 2010 (Table 2).

Table 2. Abnormal day VTEC change percentages identified from IGS stations in 2010

Time Month/Day		3/20	3/21	3/22	3/23	3/24	3/25	3/26	3/27	3/28	3/29	3/30	3/31	4/1	4/2	4/3	4/4	4/5	4/6	4/7	4/8	4/9
DECISION		C	A	C	C	A	A	A	A	C	C	C	C	A	A	C	C	A	A	A	C	A
VTEC Changes Ionospheric Percentage	AMC2						33.3							33.3	45.8	37.5		41.7	95.8	50.0		
	DRAO					33.3	66.7							50.0	66.7	70.8			91.7	58.8		
	GRAZ																	50.0	45.8	87.5	58.3	

When Table 1 and Table 2 are examined together, it is seen that the causes of VTEC anomalies are 24 March positive abnormal day (plasma intensity), 25 March positive abnormal day (solar activity, magnetic field and plasma intensity), April 1 negative abnormal day (solar activity and magnetic field), April 2 negative abnormal day (magnetic field), April 3 negative abnormal day (a calm space weather condition and is thought to be due to different effects); April 5 negative abnormal day (geomagnetic storm, geomagnetic activity and magnetic field), April 6 negative abnormal day (geomagnetic storm, geomagnetic field and magnetic field), April 7 negative abnormal day (geomagnetic storm, geomagnetic activity and magnetic field), a negative abnormal day on April 8th occurred in a calm space weather condition and is thought to be due to different effects.

5. CONCLUSIONS

When the results of the study are examined, there is a close relationship between the anomalies occurring in ionospheric TEC changes and the changes detected from indices of space weather conditions. The averages of the calculated ionospheric TEC anomaly percentages were compared and evaluated with respect to equatorial and mid-latitude generations. When the averages of percentage values of anomalies and TEC changes occurring in the mid-latitude and equatorial latitudes are separately calculated, the average of the ionospheric TEC anomalies in the mid-latitude zone was 50.4% TECU, and the average of the anomalies in the equatorial zone was 43.3% TECU. Taking these changes into consideration, it is seen that the ionospheric TEC anomaly changes in the mid-latitudes are higher than those of the equatorial basin. The investigations revealed that it is possible to use the GPS-TEC for monitoring the space weather conditions. With the new technology will take place in satellite and space techniques to analyze the changes occurring in our world will be much easier. This study also provided a basis for the investigation of ionospheric anomalies before the earthquakes. In the future these considerations will be overseen by new statistical methods.

ACKNOWLEDGMENT

The authors would like to thank, the CDDIS (Crustal Dynamics Data and Information System) data and products archive, for providing the RINEX, SP3 and IONEX files, the NASA Space Flight Center Space Physics Data Facility and the University of Southern California Space Science Center for providing changes to space weather condition indices. Special thanks to TUBITAK CAYDAG for supporting our project with the grant no. 116Y109.

REFERENCES

Abraha, G., 2014. Total Electron Content (TEC) Variability of Low Latıtude Ionosphere and Role of Dynamical Coupling: Quıet and Storm-Time Characteristics, PhD Thesis, Addis Ababa University Addis Ababa, Ethiopia.

Adeyini, E., O., 1986. Magnetic Storm Effects on the Morphology of the Equatorial F2-Layer, Journal of Atmospheric and Terrestrial Physics, 48, 8, 695-702.

Aschwanden, M., J., 2005. Physics of the Solar Corona an Introduction with Problems and Solutions, Sprınger-Praxis Books in Astronomy and Planetary Sciences, Springer-Verlag Berlin Heidelberg, New York, 908.

Contadakis, M., Arabelos, D., Pikridas, C. and Spatalas, S., 2012. Total Electron Content Variations over Southern Europe before and during the M 6.3 Abruzzo Earthquake of April 6, 2009, Annals of Geophysics, 55, 83-93.

De Canck, M., H., 2007. Ionosphere Properties and Behaviors, Antennex, 119, 6-7.

Durmaz, M. and Karslioglu, M., O., 2014. Regional Vertical Total Electron Content (VTEC) Modeling Together with Satellite and Receiver Differential Code Biases (DCBs) Using Semi-Parametric Multivariate Adaptive Regression B-splines (SP-BMARS), J Geod., 89, 4, 347-360.

Gonzalez, W., D., Joselyn, J., A., Kamide, Y., Kroehl, H., W., Rostoker, G., Tsurutani, B., T. and Vasyliunas, V., M., 1994. What is a geomagnetic storm? J. Geophys. Res., 99, 5771-5792.

Hawarey, M. and Ayan, T., 2004. Uzay Mekiği Tırmanışı, Deprem, ve Füze Fırlatılışından Kaynaklanan TEC Değişimlerinin GPS ile Belirlenmesi, İTÜ Dergisi, 3, 2-3-4-5, 45-56.

Jin, R., Jin, S., G. and Feng, G., P., 2012. M_DCB: Matlab Code for Estimating GNSS Satellite and Receiver Differential Code Biases, GPS Solut., 16,4, 541-548.

Kamide, Y., Yokoyama, N., Gonzalez, W., Tsurutani, B. T., Daglis, I. A., Brekke, A. and Masuda, S., 1998. Two-Step Development of Geomagnetic Storms, Journal of Geophysical Research-Space Physics, 103, 6917-6921.

Klobuchar, J., A., 1986. Design and Characteristics of the GPS Ionospheric Time-Delay Algorithm for Single-Frequency Users, In: Procedings of the IEEE Position Location and Navigation Symposium, Las Vegas.

Klotz, S., and Johnson, N., L., (Eds.), 1983. Encyclopedia of Statistical Sciences, John Wiley and Sons.

Komjathy, A., 1997. Global Ionospheric Total Electron Content Mapping Using the Global Positioning System, Ph.D. Thesis, Dept. of Geodesy and Geomatics Engineering Technical Report No. 188. Univ. of New Brunswick, Fredericton, New Brunswick, Canada.

Lanyi, G., E. and Roth, T., 1988. A Comparison of Mapped and Measured Total Ionospheric Electron Content Using Global Positioning System and Beacon Satellite Observations, Radio Sci., 23, 483-492.

Liu, J., Y., Chen, Y., I., Chen, C., H., Liu, C., Y., Chen, C., Y., Nishihashi, M., Li, J., Z., Xia, Y., Q., Oyama, K., I., Hattori, K. and Lin, C., H., 2009. Seismo Ionospheric GPS Total Electron Content Anomalies Observed before The 12 May 2008 Mw 7.9 Wenchuan Earthquake, Journal of Geophysical Research-Space Physics, 114.

Liu, M., Luo, G. and Wang, H., 2014. The 2013 Lushan earthquake in China Tests Hazard Assessments, Seismol. Res. Lett., 85, 1, 40-43.

Loewe, C., A. and Prölss, G., W., 1997. Classification and Mean Behavior of Magnetic Storms, Journal of Geophysical Research, 102, A7, 14, 209-213.

Melnikov, V.F., 1990. Relationships between Microwave, Hard X-Ray, and Corpusclar Emissions of Solar Flares, PhD Thesis, Radiophysical Research Institute, Nizhniy Novgorod, Russia.

Prölss, G., 2004. In Physics of the Earth's Space Environment: An Introduction, Springer Berlin / Heidelberg, 513.

Ratcliffe, J., A., 1972. An Introduction to the Ionosphere and Magnetosphere, Cambridge University Press, 256.

Rishbeth, H. and Garriott, O., K., 1969. Introduction to Ionospheric Physics, Elsevier, New York, 335.

Rozhnoi, A., Solovieva, M., S., Molchanov, O., A. and Hayakawa, M., 2004. Middle Latitude LF (40 kHz) Phase Variations Associated with Earthquakes for Quiet and Disturbed Geomagnetic Conditions, Physics and Chemistry of the Earth, 29, 589-598.

Schaer, S., 1999. Mapping and Predicting the Earth's Ionosphere Using the Global Positioning System, PhD Thesis, Geodatisch-geophysikalische Arbeiten in der Schweiz, Vol. 59.

Schwenn, R., 2001. Solar Wind: Global Properties, Encyclopedia of Astronomy and Astrophysics, Institute of Physics Publishing, Dirac House, Temple Back, Bristol, BS1 6BE, UK.

Tobiska, W., K., 1996. Current Status of Solar EUV Measurements and Modeling, Adv. Space Res., 18, 3-10.

Turunen, T. and Rao, M., M., 1980. Examples of the Influence of Strong Magnetic Storms on the Equatorial F-layer, Journal of Atmospheric and Terrestrial Physics, 42, 323-330.

URL-1, http://www.spaceweather.ca/sbg-en.php Space Weather Conditions. 22 March 2014.

URL-2, http://omniweb.gsfc.nasa.gov/html/ow_data.html#7 Proton Flux. 24 March 2014.

URL-3, http://www.swpc.noaa.gov/impacts/hf-radio-communications Radio Signals. 28 March 2014.

URL-4, http://www.carnicominstitute.org/articles/solar1.htm Proton Density 29 March 2014.

URL-5, http://www.spaceweather.ca/solarflux/sx-1-en.php Solar Flux Indice (F10.7cm). 30 March 2014.

URL-6, http://www.swpc.noaa.gov/phenomena/solar-euv-irradiance EUV Flares on Sun. 1 April 2014.

URL-7, http://www.usc.edu/dept/space_science/semdatafolder/semdownload.htm EUV Flux (0.1-50 nm and 26-34 nm) 17 August 2014.

URL-8, http://omniweb.gsfc.nasa.gov/form/dx1.html Space Weather Indices data web interface. 17 August 2014.

URL-9, https://igscb.jpl.nasa.gov/components/prods.html The Accuracy of TEC Estimates on the IGS-Calculated Continents. 30 July 2014.

Vellinov, P., I., Spasssov, Chr. W. and Kolev, S., I., 1992. Ionospheric Effects of Lightning during the Increasing Part of Solar Cycle 22. Journal of Atmospheric and Terrestrial Physics, 534, 10, 1347-1353.

Vitinsky, Y., I., Kopecky, M. and Kuklin, G., V., 1986. Statistics of Sunspot Activity (in Russian), Nauka, Moscow, 397.

Wild, U., 1994. Ionosphere and Geodetic Satellite Systems: Permanent GPS Tracking Data for Modeling and Monitoring, PhD Thesis, Geodatisch-geophysikalische Arbeiten in der Schweiz, Vol. 48.

Zolesi, B. and Cander, L., R., 2014. Ionospheric Prediction and Forecasting, Springer Geophysics. ISBN 978-3-642-38429-5. Berlin: Springer-Verlag, 240.

BIOGRAPHICAL NOTES

I started my academic life first at the Department of Geomatics Engineering at Karadeniz Technical University. I completed my master degree in the Department of Mapping Engineering at Karadeniz Technical University between the years 2008-2010. In 2009 I was appointed research assistant to Harran University Department of Geomatics Engineering. I finished my Ph.D. thesis in the Department of Mapping Engineering at Karadeniz Technical University between the years 2010-2016. Currently I am working as an assistant professor at the Harran University.

CONTACTS

Mustafa ULUKAVAK
Harran University
Harran Üniversitesi Osmanbey Kampüsü Mühendislik Fakültesi Harita Mühendisliği Bölümü
63300, Şanlıurfa
TÜRKİYE
Tel. +90 414 3183000-1693
Fax +90 414 3183190
Email:mulukavak@gmail.com
Web site: http://akademik.yok.gov.tr/AkademikArama/AkademisyenGorevOgrenimBilgileri?islem=direct&authorId=78C149AA01B2D92E